Shear wave reflectivity imaging of the Nazca-South America subduction zone: Stagnant slab in the mantle transition zone?

Sean Contenti,[1] Yu Jeffrey Gu,[1] Ahmet Ökeler,[2] and Mauricio D. Sacchi[1]

Received 18 October 2011; revised 21 December 2011; accepted 27 December 2011; published 31 January 2012.

[1] In this study we utilize over 5000 SS waveforms to investigate the high-resolution mantle reflectivity structure down to 1200 km beneath the South American convergent margin. Our results indicate that the dynamics of the Nazca subduction are more complex than previously suggested. The 410- and 660-km seismic discontinuities beneath the Pacific Ocean and Amazonian Shield exhibit limited lateral depth variations, but their depths vary substantially in the vicinity of the subducting Nazca plate. The reflection amplitude of the 410-km discontinuity is greatly diminished in a ∼1300-km wide region in the back-arc of the subducting plate, which is likely associated with a compositional heterogeneity on top of the upper mantle transition zone. The underlying 660-km discontinuity is strongly depressed, showing localized depth and amplitude variations both within and to the east of the Wadati-Benioff zone. The width of this anomalous zone (∼1000 km) far exceeds that of the high-velocity slab structure and suggesting significant slab deformation within the transition zone. The shape of the 660-km discontinuity and the presence of lower mantle reflectivity imply both stagnation and penetration are possible as the descending Nazca slab impinges upon the base of the upper mantle. **Citation:** Contenti, S., Y. J. Gu, A. Ökeler, and M. D. Sacchi (2012), Shear wave reflectivity imaging of the Nazca-South America subduction zone: Stagnant slab in the mantle transition zone?, *Geophys. Res. Lett.*, *39*, L02310, doi:10.1029/2011GL050064.

1. Introduction

[2] The Nazca plate has been subducting under the western margin of the South American continent since at least the late Cretaceous period [*Pardo-Casas and Molnar*, 1987]. This long-lasting ocean-continent convergence, which is ongoing at a present-day rate of ∼6.6 cm/yr [*Kendrick et al.*, 2003], is directly responsible for the formation of the Andean mountain chain and the associated seismic/volcanic activity along the Wadati-Benioff zone [*Cahill and Isacks*, 1992]. The substantial surface topography of the region is mirrored by complexities in subduction zone morphology and dynamics, as evidenced by observations from recent seismic tomographic analyses [*Engdahl et al.*, 1995; *Li et al.*, 2008; *Fukao et al.*, 2009]. Continuous high velocity anomalies have been suggested to extend into the lower mantle in both northern and central South America [*Engdahl et al.*, 1995; *Li et al.*, 2008; *Fukao et al.*, 2009], whereas stagnation and/or ponding of subducted oceanic lithosphere is possible within the Mantle Transition Zone (MTZ) or at shallow lower mantle depths towards the south [*Engdahl et al.*, 1995]. Studies based on secondary reflected/converted body waves offer additional constraints on the gradients of mantle seismic velocities. A regionally depressed 660-km discontinuity has been reported by studies of SS precursors [*Flanagan and Shearer*, 1998; *Gu and Dziewoński*, 2002; *Schmerr and Garnero*, 2007] and P-to-s converted waves [*Liu et al.*, 2003; *Braunmiller et al.*, 2006; *Wölbern et al.*, 2009], which suggests a substantial low temperature anomaly near the base of the upper mantle (hereafter, all discontinuities will be referred to by d, followed by depth, e.g., *d*660). Still, constraints on mantle seismic discontinuities under the South America convergent zone have traditionally been problematic due to low data density [*Flanagan and Shearer*, 1998; *Gu et al.*, 1998, 2003], uneven sampling, and/or limited depth extent [*Liu et al.*, 2003; *Wölbern et al.*, 2009]. Recent efforts [*Schmerr and Garnero*, 2007; *Sodoudi et al.*, 2011] have shown significant improvements and future promise, though the details of the olivine phase boundaries and the nature of potential reflectors in the depth range of 300–1000 km [*Deuss and Woodhouse*, 2002] warrant further verification and discussion.

[3] In this study, we aim to provide a high-resolution analysis of mantle reflectors beneath central South America down to mid-mantle depths. Our time-to-depth conversion of an up-to-date SS precursor dataset enables a detailed regional comparison between reflection amplitudes and seismic velocity, necessary for a self-consistent model of subduction dynamics surrounding the MTZ.

2. Results

[4] We utilize over 30 years (1972–2009) of broadband and long-period earthquake waveform data with data search and processing criteria similar to that employed by *An et al.* [2007]. The resulting SS precursor dataset, which consists of 5720 seismograms, is sorted into common midpoint (CMP) gathers [*Shearer*, 1991] along the great circle arc between cross-section endpoints (Figure 1). We utilize thin rectangular bins with a dimension of 4° × 8° to maximize the nominal resolution along the dip of the Nazca slab while maintaining sufficient data in each bin for effective noise suppression. The data in the cross section are then time shifted to account for crustal thickness (CRUST2.0 [*Bassin and Laske*, 2000]), surface topography (ETOPO2 [*National Geophysical Data Center*, 1998]), and mantle heterogeneities (S12WM13 [*Su et al.*, 1994]). The corrected seismograms in each bin are subsequently converted from time to depth using PREM predicted travel times [*Dziewoński*

[1]Department of Physics, University of Alberta, Edmonton, Alberta, Canada.
[2]Department of Earth and Planetary Sciences, Harvard University, Cambridge, Massachusetts, USA.

0094-8276/12/2011GL050064

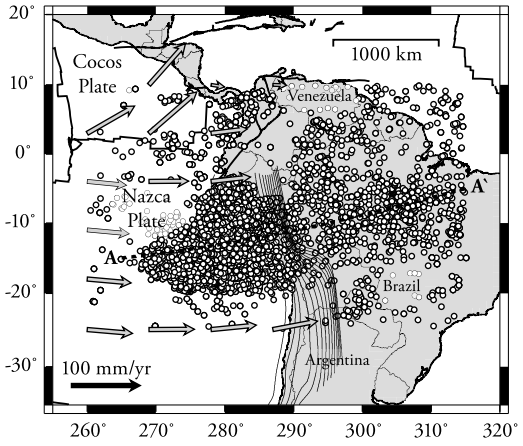

Figure 1. Midpoints of the 5720 seismograms used in this study, along with GPS plate motion vectors from the GSRM-1 model (filled arrows) [*Kreemer et al.*, 2003]. Slab contours are obtained from the Regionalized Upper Mantle (RUM) model of *Gudmundsson and Sambridge* [1998] (thin grey lines). The plate boundaries are plotted after *Bird* [2003] (thin black lines) and the surface trace of the cross section are represented using a thick black line.

and Anderson, 1981]. To eliminate structures with large uncertainties, we produce a cross section of reflectivity energy above the 95% confidence interval by subtracting two standard deviations of the bootstrap uncertainty [*Efron and Tibshirani*, 1991; *An et al.*, 2007] from the depth-converted reflectivity data. A detailed overview of our data and methodology is included in the auxiliary material.[1]

[5] Figure 2 shows the high-resolution reflectivity image constructed from SS precursors bottoming beneath the study region. The mantle beneath the western segment (5°–20° along path) is dominated by five sub-horizontal reflectors at approximate depths of 300, 420, 520, 660, and 900 km. The MTZ reflectors (*d*410, *d*520, *d*660) in this region show minimal depth variation, with all three reflectors residing near the respective global averages. Broad, laterally coherent mantle reflections observed east of the Nazca-South America subduction zone are similar in character to those beneath the Pacific Ocean. The 410-km discontinuity is depressed down to 430 km while *d*660 is relatively unperturbed. Intermittent reflections from *d*520 are visible at 45° and 47° along path at the depths of 540 and 500 km. The topography is minimal along the boundaries of the MTZ beneath the Brazilian Shield (35°–40° along path), with the exception of a gradual shallowing (by <10 km) of *d*410 beneath the Brazilian Shield at 305° longitude.

[6] The mantle under the Andean convergent zone (22°–35°) is considerably more complex than within the adjacent tectonic domains (Figure 2a). Beneath the Andes, *d*410 increases slightly in amplitude and undergoes ~10 km of uplift relative to the regional average. This structure is followed by a wide (~15°) reflection gap in the back-arc of the subduction zone, where the amplitude of *d*410 is reduced to <3% relative to SS. Below the reflection gap (~20–30°), the base of the MTZ shows two depressed zones (by ~25 km) that are separated by areas of near-average depth and low amplitude (Figure 2a). A strong reflector with an amplitude greater than 5% is visible beneath the central Amazonian basin where the overlying *d*660 falls below our detection threshold (Figure 2a). The diffuse nature of this reflector and its considerable vertical extension (>100 km based on a 3% amplitude cutoff) argues against a sharp mantle reflection.

3. Discussions

[7] The depression of *d*410 below the Brazilian Shield [*Schmerr and Garnero*, 2007], could result from a hot thermal anomaly. Due to the lack of corresponding uplift on d660, the associated temperature variations are most likely confined to the upper mantle. Despite limited evidence from global tomographic models shown in Figures 2b and 2c, a low velocity zone has been suggested by regional tomographic models [*VanDecar et al.*, 1995] and interpreted as evidence of a fossil plume beneath the Parana flood basalt province. The insulating effects of a thick cratonic root, which may impede heat flow in the region, could also cause a broad depression of *d*410 below central/eastern South America.

[8] The modest uplift of *d*410 in the Wadati-Benioff zone of the descending slab is expected due to the positive Clapeyron slope of the olivine to wadsleyite ($\alpha \rightarrow \beta$) phase transformation [*Bina and Helffrich*, 1994]. The presence of subducted oceanic lithosphere in the MTZ is further corroborated by the 7 km depression of *d*660 relative to the regional average. Assuming a pyrolitic mantle composition with 10% iron [*Ringwood*, 1975], this topographic low corresponds to a local temperature decrease of 120°C [*Bina and Helffrich*, 1994] surrounding the ringwoodite to perovskite + magnesiowustite ($\gamma \rightarrow pv + mw$) transformation [*Bina and Helffrich*, 1994]. The combination of a shallow *d*410 and a deep *d*660 implies strong mantle heterogeneities down to, at the least, the base of the upper mantle beneath the convergent zone. The continuity of this structure within the MTZ is corroborated by the presence of an elevated *d*520 [*Shearer*, 1990; *Deuss and Woodhouse*, 2002] (at 500 km), which have been associated with the exothermic ($\beta \rightarrow \gamma$) phase transition [*Katsura and Ito*, 1989; *Bina and Helffrich*, 1994].

[9] The origin of a highly distinctive, ~1300 km wide reflection gap on *d*410 beneath the back-arc of the Nazca trench is debatable. While a high-temperature anomaly at the top of the MTZ could produce the observed depression, a pronounced low-velocity zone is not present in the tomographic models shown in Figures 2b and 2c. More importantly, a warm shallow mantle would increase the velocity contrast across *d*410, which is at odds with the observed amplitude reduction (Figure 2). Alternatively, incoherent stacking due to a dipping interface [*Chaljub and Tarantola*, 1997; *Neele et al.*, 1997; Y. J. Gu et al., Tracking slabs beneath northwestern Pacific subduction zones, submitted to *Earth and Planetary Science Letters*, 2011] could lower the *d*410 strength, but the 'flat' *d*410 in this region is unlikely to cause major shear-wave scattering effects. Changes in mantle composition may be required to explain the observed *d*410 reflection gap. Trench rollback to the west [*Lallemand et al.*, 2008] and the formation of a hydrated zone directly above *d*410 [*Schmerr and Garnero*, 2007] can reduce the amplitude by broadening the olivine-wadsleyite phase loop. This hydrous lens [*Zheng et al.*, 2007] has also been suggested to cause double reflections [*Schmerr and Garnero*, 2007] in

[1]Auxiliary materials are available in the HTML. doi:10.1029/2011GL050064.

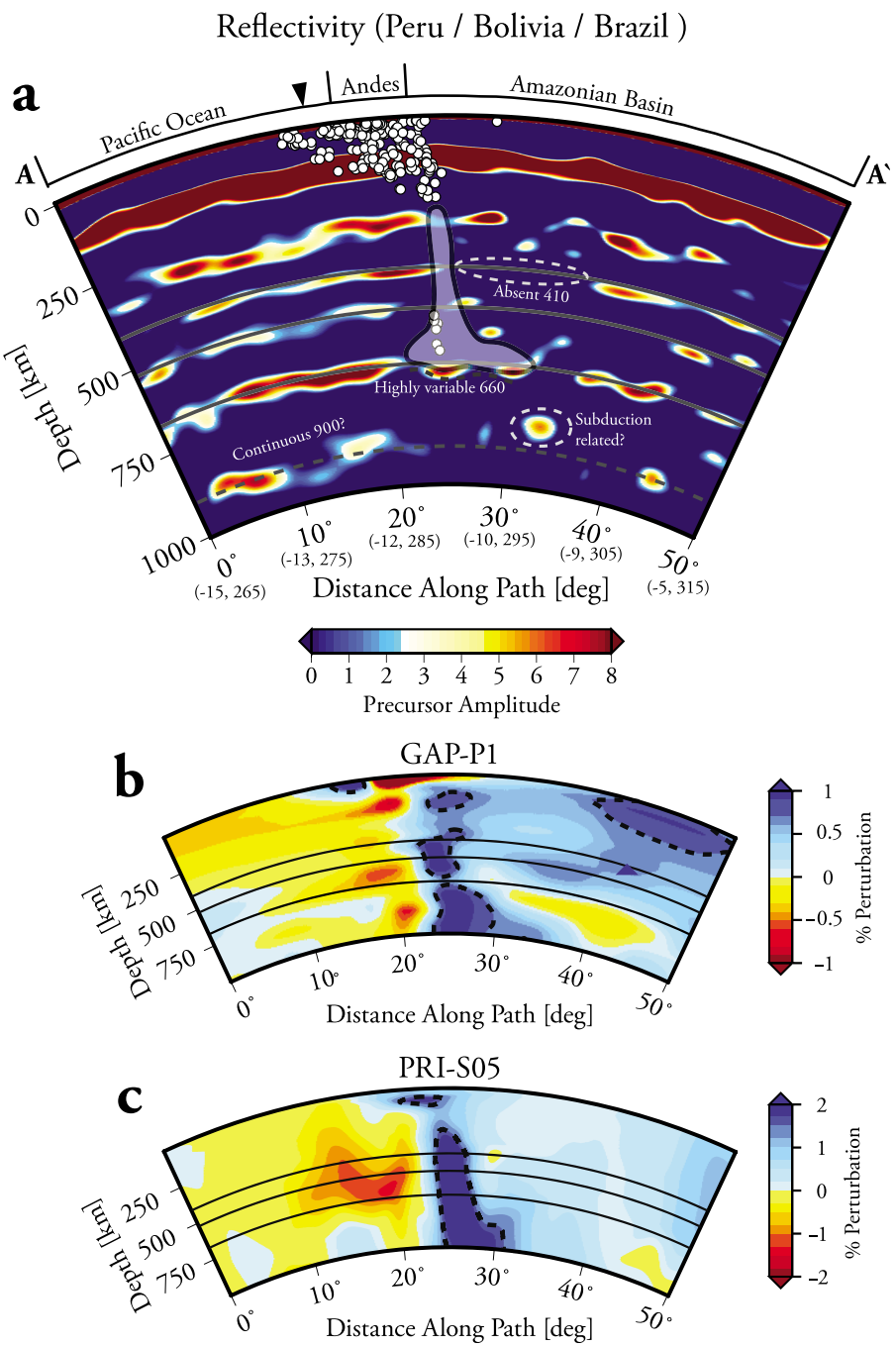

Figure 2. (a) Reflectivity cross-section across South America (see surface trace in Figure 1). The white outline shows the interpreted position of the subducting Nazca slab. The 410, 520, and 660 discontinuities are marked by black lines. Included on the horizontal axis are (latitude, longitude) coordinates corresponding to points along the great-circle arc of the cross-section. Also shown are velocity perturbation through (b) the GAP-P1 velocity model and (c) the PRI-P05 velocity model. The dashed black lines on the velocity models are the +1.5% and +0.7% velocity contours for PRI-S05 and GAP-P1, respectively. The circles indicate earthquake hypocenters along the cross-section.

response to the olivine-wadsleyite transition and the wet-dry wadsleyite boundary, although such waveform complexities appear to be more prominent in the *d*410 signals north of our study region [see *Schmerr and Garnero*, 2007] (auxiliary material). The presence of a double reflector in the vicinity of *d*410 may result in destructive interference of the scattered wave-field, leading to the appearance of a reflection gap as observed in this study. Recent numerical simulations by *Hier-Majumder and Courtier* [2011] have suggested a distributed layer of neutrally buoyant melt in the mantle between 350 and 420 km depth. Based on these models, a melt fraction of ∼1% is sufficient to explain the diminished reflection amplitude.

[10] Our observation of a deep *d*660 near the descending Nazca slab is consistent with earlier published results based on receiver functions and ScS reverberations [*Clarke et al.*,

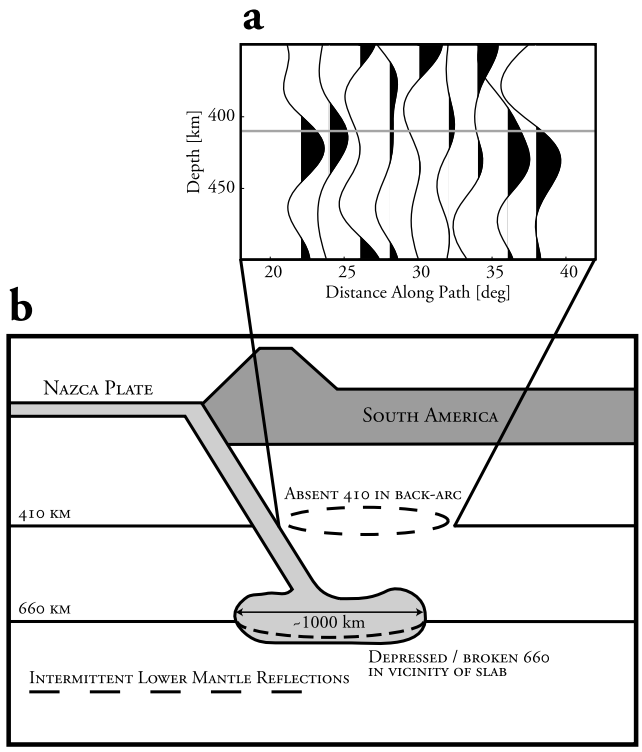

Figure 3. (a) Excerpt from the SS precursor dataset, highlighting the reflection gap on *d*410. The data includes the two bins both preceding and following the gap. (b) A schematic representation of our main results and interpretations. Entrained hydrated material forms a lens on *d*410, creating a broad zone with little to no reflection. Partial slab penetration through the bottom of the MTZ causes depression in addition to missing or significantly reduced amplitudes on *d*660. Scattered reflections in the lower mantle potentially result from deep phase transitions, or could represent direct reflections from avalanched slab material.

1995; *Liu et al.*, 2003; *Wölbern et al.*, 2009]. Due to the negative Clapeyron slope of the ringwoodite to perovskite + magnesiowustite mineral phase transition [*Bina and Helffrich*, 1994], a delayed transition is expected in a cold subducting oceanic lithosphere. The magnitude of the $\gamma \rightarrow pv + mw$ Clapeyron slope (−2.0 [*Bina and Helffrich*, 1994]) predicts a lesser deflection of *d*660 than of *d*410 (Clapeyron slope ranging from +2.5 [*Katsura and Ito*, 1989] to +4.0 [*Katsura et al.*, 2004]) under similar temperature regimes, although the opposite has been previously documented in global studies of MTZ discontinuity topography [*Gu et al.*, 1998, 2003; *Flanagan and Shearer*, 1998].

[11] The reflectivity structure at the base of the upper mantle is complex in a 1200–1500 km wide zone east of the Peru-Chile Trench. This anomalous region contains distinct zones of depression under the Andes and Amazon Basin, as well as a reflection gap beneath central Brazil (Figure 2). We interpret the unique shape of *d*660 as evidence of slab stagnation and buckling, deformation mechanisms that are likely facilitated by the high relative convergence rate of the Nazca-South America system [*Kendrick et al.*, 2003] and the observed ocean-ward migration of the Peru-Chile Trench [*Lallemand et al.*, 2008]. This interpretation (Figures 2 and 3b) is supported by recent results from reflector / converter imaging and numerical simulations of global subduction zones. Under significant trench retreat over the lifetime of a subduction zone, a mechanically 'soft' slab [*Li et al.*, 2008] could gradually settle at the base of the MTZ, as documented in the northwestern Pacific subduction system. Dynamically, a dipping slab with a relatively low viscosity compared to the surrounding mantle tends to develop into a 'spoon' or 'jellyfish' shape with relatively smooth leading edges [*Loiselet et al.*, 2010] on top of a highly viscous lower mantle [*Ribe et al.*, 2007; *Quinteros et al.*, 2010]. The 'spoon' analogy is more consistent with the interpreted shape of *d*660 in this study, where anomalous boundary variations extend well to the east of the Benioff zone. Slab stagnation near the base of upper mantle is a viable explanation. The easternmost segment of this broad zone appears to shallow toward mid MTZ depths and may provide further evidence of a highly deformed slab in the MTZ due to thermal and/or compositional variations.

[12] The distinctive reflection gap beneath the Brazil - Bolivia border remains enigmatic. Similar amplitude reduction has been documented near the Kurile-Japan arcs (Gu et al., submitted manuscript, 2011) in connection with steep boundary topography in response to substantial mass and heat fluxes across *d*660. While the reflection gap presented in this study is more distant from the Benioff zone than previously reported, waveform defocusing [*Chaljub and Tarantola*, 1997; Gu et al., submitted manuscript, 2011] due to the interaction between the leading edge of the stagnant slab and *d*660 offers a simple explanation. A potentially related structure is the strong reflector beneath the *d*660 reflection gap, which supports this interpretation and may result from avalanched oceanic lithosphere [*Tackley et al.*, 1993] near the same location. Several mechanisms have been proposed to account for this lower mantle reflector. Phase transitions in Ca-perovskite [*Stixrude et al.*, 2007], metastable garnet [*Kawakatsu and Niu*, 1994], stishovite [*Hirose et al.*, 2005] and hydrous magnesium silicates [*Ohtani*, 2005; *van der Meijde et al.*, 2003; *Courtier and Revenaugh*, 2006] all occur within the depth range of the observed lower mantle reflector. On the other hand, slab-centric interpretations of the aforementioned lower mantle reflector remain questionable for two key reasons: 1) relatively large data uncertainty in the vicinity of the *d*660 gap, and 2) consistent reflections at 800–950 km depth away from the Benioff zone, particularly beneath the Pacific ocean in the distance range of 0°–25° along profile. A chemical stratification [*Wen and Anderson*, 1997] cannot be ruled out as a plausible explanation for the semi-continuous lower mantle interface at 800–950 km depth.

4. Conclusions

[13] Our SS-precursor analysis has revealed a sharp contrast between the simple reflectivity structures in relatively undisturbed tectonic regimes and structure observed in regions of ongoing subduction. In the back-arc of the Nazca subduction, we observe a ∼1300 km wide reflection gap on *d*410. This highly anomalous structure is likely associated with compositional anomalies at the top of the MTZ, although the exact mechanism remains uncertain. Strong depressions are observed near the base of the MTZ within and to the east of the Wadati-Benioff zone. The shape and width (∼1000 km)

of this anomaly suggest structural complexities of the subducting Nazca plate beyond a simple form of penetration. The Nazca slab likely undergoes significant deformation within the MTZ, resulting in pockets of stagnated lithospheric material at the base of the upper mantle. Finally, we identify anomalous reflectors beneath the Benioff zone. While this observation could be caused by subducted ocean lithosphere within the shallow lower mantle, laterally coherent reflectors identified in the depth range of 800–950 km, particularly beneath the Nazca plate, require further explanations.

[14] **Acknowledgments.** We are grateful to Rafaella Montelli and Masayuki Obayashi for use of their global seismic velocity models. Comments from two anonymous reviewers have greatly improved the paper. Many of the figures were generated using the Generic Mapping Tools (GMT) [*Wessel and Smith*, 1998]. This project is funded by the National Science and Engineering Research Council (NSERC) of Canada and the University of Alberta.

[15] The Editor thanks two anonymous reviewers for their assistance in evaluating this paper.

References

An, Y., Y. J. Gu, and M. D. Sacchi (2007), Imaging mantle discontinuities using least squares Radon transform, *J. Geophys. Res.*, *112*, B10303, doi:10.1029/2007JB005009.

Bassin, C., and G. Laske (2000), The current limits of resolution for surface wave tomography in North America, *Eos. Trans. AGU*, *81*(48), Fall Meet. Suppl., Abstract S12A-03.

Bina, C. R., and G. Helffrich (1994), Phase transition Clapeyron slopes and transition zone seismic discontinuity topography, *J. Geophys. Res.*, *99*(B8), 15,853–15,860, doi:10.1029/94JB00462.

Bird, P. (2003), An updated digital model of plate boundaries, *Geochem. Geophys. Geosyst.*, *4*(3), 1027, doi:10.1029/2001GC000252.

Braunmiller, J., S. van der Lee, and L. Doermann (2006), Mantle transition zone thickness in the Central South-American Subduction Zone, in *Earth's Deep Water Cycle*, *Geophys. Monogr. Ser.*, vol. 168, edited by S. D. Jacobsen and S. van der Lee, pp. 215–224, AGU, Washington, D. C., doi:10.1029/168GM16.

Cahill, T., and B. L. Isacks (1992), Seismicity and shape of the subducted Nazca Plate, *J. Geophys. Res.*, *97*(B12), 17,503–17,529.

Chaljub, E., and A. Tarantola (1997), Sensitivity of SS precursors to topography on the upper-mantle 660-km discontinuity, *Geophys. Res. Lett.*, *24*(21), 2613–2616, doi:10.1029/97GL52693.

Clarke, T. J., P. G. Silver, Y. Yeh, D. E. James, T. C. Wallace, and S. L. Beck (1995), Close in ScS and sScS reverberations from the 9 June 1994 Bolivian earthquake, *Geophys. Res. Lett.*, *22*(16), 2313–2316, doi:10.1029/95GL02062.

Courtier, A. M., and J. Revenaugh (2006), A water-rich transition zone beneath the eastern United States and Gulf of Mexico from multiple ScS reverberations, in *Earth's Deep Water Cycle*, *Geophys. Monogr. Ser.*, vol. 168, edited by S. D. Jacobsen and S. van der Lee, pp. 181–193, AGU, Washington, D. C., doi:10.1029/168GM14.

Deuss, A., and J. H. Woodhouse (2002), A systematic search for mantle discontinuities using SS-precursors, *Geophys. Res. Lett.*, *29*(8), 1249, doi:10.1029/2002GL014768.

Dziewoński, A. M., and D. L. Anderson (1981), Preliminary reference Earth model, *Phys. Earth Planet. Inter.*, *25*(4), 297–356, doi:10.1016/0031-9201(81)90046-7.

Efron, B., and R. Tibshirani (1991), Statistical data analysis in the computer age, *Science*, *253*(5018), 390–395, doi:10.1126/science.253.5018.390.

Engdahl, E. R., R. D. van der Hilst, and J. Berrocal (1995), Imaging of subducted lithosphere beneath South America, *Geophys. Res. Lett.*, *22*(16), 2317–2320.

Flanagan, M. P., and P. M. Shearer (1998), Global mapping of topography on transition zone velocity discontinuities by stacking SS precursors, *J. Geophys. Res.*, *103*(B2), 2673–2692.

Fukao, Y., M. Obayashi, T. Makakuki, and the Deep Slab Project Group (2009), Stagnant slab: A review, *Annu. Rev. Earth Planet. Sci.*, *37*, 19–46.

Gu, Y., A. M. Dziewoński, and C. B. Agee (1998), Global de-correlation of the topography of transition zone discontinuities, *Earth Planet. Sci. Lett.*, *157*(1–2), 56–67, doi:10.1016/S0012-821X(98)00027-2.

Gu, Y. J., and A. M. Dziewonski (2002), Global variability of transition zone thickness, *J. Geophys. Res.*, *107*(B7), 2135, doi:10.1029/2001JB000489.

Gu, Y. J., A. M. Dziewoński, and G. Ekström (2003), Simultaneous inversion for mantle shear velocity and topography of transition zone discontinuities, *Geophys. J. Int.*, *154*, 559–583.

Gudmundsson, Ó., and M. Sambridge (1998), A regionalized upper mantle (RUM) seismic model, *J. Geophys. Res.*, *103*(B4), 7121–7136, doi:10.1029/97JB02488.

Hier-Majumder, S., and A. Courtier (2011), Seismic signature of small melt fraction atop the transition zone, *Earth Planet. Sci. Lett.*, *308*(3–4), 34–342, doi:10.1016/j.epsl.2011.05.055.

Hirose, K., N. Takafuji, N. Sata, and Y. Ohishi (2005), Phase transition and density of subducted MORB crust in the lower mantle, *Earth Planet. Sci. Lett.*, *237*(1–2), 239–251, doi:10.1016/j.epsl.2005.06.035.

Katsura, T., and E. Ito (1989), The system Mg_2SiO_4-Fe_2SiO_4 at high pressures and temperatures: Precise determination of stabilities of olivine, modified spinel, and spinel, *J. Geophys. Res.*, *94*(B11), 15,663–15,670, doi:10.1029/JB094iB11p15663.

Katsura, T., et al. (2004), Olivine-wadsleyite transition in the system $(Mg, Fe)_2SiO_4$, *J. Geophys. Res.*, *109*, B02209, doi:10.1029/2003JB002438.

Kawakatsu, H., and F. Niu (1994), Seismic evidence for a 920-km discontinuity in the mantle, *Nature*, *371*, 301–305, doi:10.1038/371301a0.

Kendrick, E., M. Bevis, R. Smalley Jr., B. Brooks, R. B. Vargas, E. Lauria, and L. P. S. Fortes (2003), The Nazca-South America Euler vector and its rate of change, *J. South Am. Earth Sci.*, *16*(2), 125–131, doi:10.1016/S0895-9811(03)00028-2.

Kreemer, C., W. E. Holt, and A. J. Haines (2003), An integrated global model of present-day plate motions and plate boundary deformation, *Geophys. J. Int.*, *154*(1), 8–34, doi:10.1046/j.1365-246X.2003.01917.x.

Lallemand, S., A. Heuret, C. Faccenna, and F. Funiciello (2008), Subduction dynamics as revealed by trench migration, *Tectonics*, *27*, TC3014, doi:10.1029/2007TC002212.

Li, C., R. D. van der Hilst, E. R. Engdahl, and S. Burdick (2008), A new global model for P wave speed variations in Earth's mantle, *Geochem. Geophys. Geosyst.*, *9*, Q05018, doi:10.1029/2007GC001806.

Liu, K. H., S. S. Gao, P. G. Silver, and Y. Zhang (2003), Mantle layering across central South America, *J. Geophys. Res.*, *108*(B11), 2510, doi:10.1029/2002JB002208.

Loiselet, C., J. Braun, L. Husson, C. Le Carlier de Veslud, C. Thieulot, P. Yamato, and D. Grujic (2010), Subducting slabs: Jellyfishes in the Earth's mantle, *Geochem. Geophys. Geosyst.*, *11*, Q08016, doi:10.1029/2010GC003172.

National Geophysical Data Center (1998), Digital relief of the surface of the Earth, *Data Announce. 88-MGG-02*, NOAA, Boulder, Colo.

Neele, F., H. de Regt, and J. VanDecar (1997), Gross errors in upper-mantle discontinuity topography from underside reflection data, *Geophys. J. Int.*, *129*, 194–204.

Ohtani, E. (2005), Water in the mantle, *Elements*, *1*(1), 25–30.

Pardo-Casas, F., and P. Molnar (1987), Relative motion of the Nazca (Farallon) and South American Plates since Late Cretaceous time, *Tectonics*, *6*(3), 233–248.

Quinteros, J., S. V. Sobolev, and A. A. Popov (2010), Viscosity in transition zone and lower mantle: Implications for slab penetration, *Geophys. Res. Lett.*, *37*, L09307, doi:10.1029/2010GL043140.

Ribe, N., E. Stutsmann, Y. Ren, and R. van der Hilst (2007), Buckling instabilities of subducted lithosphere beneath the transition zone, *Earth Planet. Sci. Lett.*, *254*(1–2), 173–179, doi:10.1016/j.epsl.2006.11.028.

Ringwood, A. E. (1975), *Composition and Petrology of the Earth's Mantle*, McGraw-Hill, New York.

Schmerr, N., and E. J. Garnero (2007), Upper mantle discontinuity topography from thermal and chemical heterogeneity, *Science*, *318*(5850), 623–626, doi:10.1126/science.1145962.

Shearer, P. M. (1990), Seismic imaging of upper-mantle structure with new evidence for a 520-km discontinuity, *Nature*, *344*, 121–126, doi:10.1038/344121a0.

Shearer, P. M. (1991), Constraints on upper mantle discontinuities from observations of long-period reflected and converted phases, *J. Geophys. Res.*, *96*(B11), 18,147–18,182.

Sodoudi, F., X. Yuan, G. Asch, and R. Kind (2011), High-resolution image of the geometry and thickness of the subducting Nazca lithosphere beneath northern Chile, *J. Geophys. Res.*, *116*, B04302, doi:10.1029/2010JB007829.

Stixrude, L., C. Lithgow-Bertelloni, B. Kiefer, and P. Fumagalli (2007), Phase stability and shear softening in $CaSiO_3$ perovskite at high pressure, *Phys. Rev. B*, *75*, 024108, doi:10.1103/PhysRevB.75.024108.

Su, W., R. L. Woodward, and A. M. Dziewonski (1994), Degree 12 model of shear velocity heterogeneity in the mantle, *J. Geophys. Res.*, *99*(B4), 6945–6980, doi:10.1029/93JB03408.

Tackley, P. J., D. J. Stevenson, G. A. Glatzmaier, and G. Schubert (1993), Effects of an endothermic phase transition at 670 km depth in a spherical model of convection in the Earth's mantle, *Nature*, *361*, 699–704, doi:10.1038/361699a0.

VanDecar, J. C., D. E. James, and M. Assumpção (1995), Seismic evidence for a fossil mantle plume beneath South America and implications for plate driving forces, *Nature*, *378*, 25–31.

van der Meijde, M., F. Marone, D. Giardini, and S. van der Lee (2003), Seismic evidence for water deep in Earth's upper mantle, *Science*, *300*, 1556–1558, doi:10.1126/science.1083636.

Wen, L., and D. L. Anderson (1997), Layered mantle convection: A model for geoid and topography, *Earth Planet. Sci. Lett.*, *146*(3–4), 367–377, doi:10.1016/S0012-821X(96)00238-5.

Wessel, P., and W. H. F. Smith (1998), New, improved version of Generic Mapping Tools released, *Eos Trans. AGU*, *79*(47), 579.

Wölbern, I., B. Heit, X. Yuan, G. Asch, R. Kind, J. Viramonte, S. Tawackoli, and H. Wilke (2009), Receiver function images from the Moho and the slab beneath the Altiplano and Puna plateaus in the central Andes, *Geophys. J. Int.*, *177*(1), 296–308, doi:10.1111/j.1365-246X.2008.04075.x.

Zheng, Y., T. Lay, M. P. Flanagan, and Q. Williams (2007), Pervasive seismic wave reflectivity and metasomatism of the Tonga mantle wedge, *Science*, *316*(5826), 855–859, doi:10.1126/science.1138074.

S. Contenti, Y. J. Gu, and M. D. Sacchi, Department of Physics, University of Alberta, 4-183 CCIS, Edmonton, AB T6G 2E1, Canada. (contenti@ualberta.ca)

A. Ökeler, Department of Earth and Planetary Sciences, Harvard University, Hoffman Lab, 20 Oxford St., Cambridge, MA 02138, USA.